A Simplified Transmission-Line Based Crosstalk Noise Model for On-Chip RLC Wiring

Kanak Agarwal
University of Michigan
agarwalk@umich.edu

Dennis Sylvester
University of Michigan
dennis@eecs.umich.edu

David Blaauw
University of Michigan
blaauw@umich.edu

Abstract - In this paper, we present a new RLC crosstalk noise model that combines simplicity, accuracy, and generality. The new model is based on transmission line theory and is applicable to asymmetric driver and line configurations. The results show that the model captures both the waveform shape and peak noise accurately (average error in peak noise was 6.5%). A key feature of the new model is that its derivation and form enables physical insight into the dependency of total coupling noise on relevant physical design parameters. The model is applied to investigate the impact of various physical design optimizations (e.g., wire sizing and spacing, shield insertion) on total RLC coupled noise. Results indicate that common (capacitive) noise avoidance techniques can behave quite differently when both capacitive and inductive coupling are considered together.

I. Introduction

On-chip inductance has become significant in designs with GHz clock frequencies [1,2]. One aspect of on-chip inductance that has not been studied well is mutual inductive coupling. Mutual inductance causes signal integrity issues by injecting noise pulses on a victim line. The injected noise can either cause functional failure or change the delay of the victim line [3].

Most existing noise models and avoidance techniques consider only capacitive coupling [4]. However, at current operating frequencies inductive crosstalk effects can be substantial and should be included for complete coupling noise analysis. Figure 1 shows noise waveforms for two fully coupled lines (in this case minimum spacing is used along with a larger linewidth for RC delay reduction as may be done for critical global signals). The figure also shows waveforms for capacitive and inductive coupling noise separately.[1] The waveforms show that inductive noise can be comparable in magnitude to the noise due to capacitive coupling and hence neglecting inductance in noise analysis can be highly inaccurate.

Recently, there has been work that includes inductive coupling in noise modeling. A noise model for two coupled RLC lines was proposed in [5]; however, this model is only applicable to loosely coupled lines for which mutual inductance and coupling capacitance are much smaller than self-inductance and ground capacitance respectively. This approximation is not valid for on-chip interconnects where the ratio of coupling capacitance to ground capacitance can easily exceed one and similarly the ratio of mutual inductance to self inductance can be in the range of 0.7 to 0.8 [6]. Another model for coupled RLC interconnects was proposed in [7]. The model maps two coupled lines to two isolated single lines and then approximates each isolated line as a one-segment RLC pi circuit. One disadvantage of this approach is

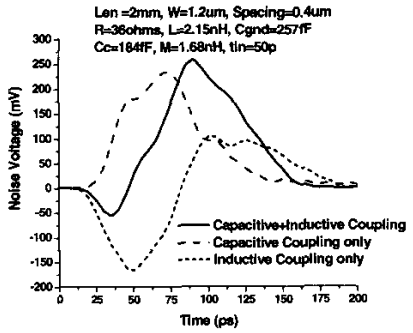

Fig 1: Noise waveforms for capacitive, inductive and capacitive + inductive coupling for two coupled lines.

that it is applies only to identical wires with identical drivers. Furthermore, its use of a simple lumped one-segment pi approximation makes it invalid for fast transition times. At current frequencies, on-chip interconnects act as lossy transmission lines. Hence, single-lump approximations for noise modeling are insufficient since transmission line effects such as time of flight and reflections must be considered. Reference [8] proposes a model based on the rigorous solution of coupled distributed RLC lines but the model is extremely complex and as such does not provide useful insight for physical design noise optimizations.

In this paper, we propose a transmission line based coupling noise model that is simple while retaining accuracy. Due to its simplicity, the model is useful in understanding noise waveform shapes due to capacitive and inductive coupling and also their dependencies on various parameters. The model can handle asymmetric line and driver configurations. The proposed model will be particularly useful in investigating the effect of physical design changes (linewidth, spacing, shield insertion, etc.) on total (capacitive and inductive) noise.

The remainder of the paper is organized as follows. We begin by reviewing relevant transmission line theory in the following section. The second section also presents our approach to modeling RLC coupling noise waveforms. In Section 3, we validate the new model by comparing to SPICE results. Using this model, we examine the effects of various physical design optimizations on RLC noise in Section 4 before concluding in Section 5.

II. Coupling Noise Model

In this section, we first review transmission line theory for two coupled lines and then develop a new noise model based on this theory.

A. *Coupled Transmission Line Theory*

Consider two distributed coupled RLC lines. Let R, L, and C be the line resistance, self-inductance, and ground capacitance per unit length of the line respectively. The lines are capacitively and inductively coupled. Let C_C be the per unit length coupling

[1] The capacitive coupling noise waveform is generated by setting mutual inductance to zero and similarly inductive coupling noise is generated by setting coupling capacitance to the ground capacitance. Note that the capacitive coupling noise waveform is not smooth due to the line self inductance.

This work is supported by National Science Foundation Career grant no. CCR-0133401 and by equipment donations from Intel Corporation and Sun Microsystems.

0-7803-8175-0/04/$17.00 ©2004 IEEE.

capacitance and M be the per unit length mutual inductance between the lines. At any point z along the line, the voltage and current waveforms on line 1 and line 2 satisfy following set of differential equations.

$$-\frac{\partial V_1}{\partial z} = (R+sL)I_1 + sMI_2 \quad -\frac{\partial I_1}{\partial z} = s(C+C_C)V_1 - sC_CV_2 \tag{1}$$
$$-\frac{\partial V_2}{\partial z} = (R+sL)I_2 + sMI_1 \quad -\frac{\partial I_2}{\partial z} = s(C+C_C)V_2 - sC_CV_1$$

Here, $V_1(z,t)$, $I_1(z,t)$ and $V_2(z,t)$, $I_2(z,t)$ are voltage and current waveforms on lines 1 and 2 respectively. The generic solution of the above set of equations is given by

$$\begin{aligned} V_1 &= (A_1e^{-\gamma_e z} + A_2e^{\gamma_e z}) + (A_3e^{-\gamma_o z} + A_4e^{\gamma_o z}) \\ V_2 &= (A_1e^{-\gamma_e z} + A_2e^{\gamma_e z}) - (A_3e^{-\gamma_o z} + A_4e^{\gamma_o z}) \\ I_1 &= \frac{1}{Z_{Oe}}(A_1e^{-\gamma_e z} - A_2e^{\gamma_e z}) + \frac{1}{Z_{Oo}}(A_3e^{-\gamma_o z} - A_4e^{\gamma_o z}) \\ I_2 &= \frac{1}{Z_{Oe}}(A_1e^{-\gamma_e z} - A_2e^{\gamma_e z}) - \frac{1}{Z_{Oo}}(A_3e^{-\gamma_o z} - A_4e^{\gamma_o z}) \end{aligned} \tag{2}$$

Here, the A_i's are constants whose values are obtained from the boundary conditions. The constants γ_e and γ_o are defined as *even* and *odd mode* propagation constants [9]. These constants are given by

$$\begin{aligned} \gamma_e &= \sqrt{sC[R+s(L+M)]} \\ \gamma_o &= \sqrt{s(C+2C_C)[R+s(L-M)]} \end{aligned} \tag{3}$$

Similarly, Z_{0e} and Z_{0o} are defined as even and odd mode characteristic impedances and can be expressed as

$$\begin{aligned} Z_{0e} &= \sqrt{\frac{R+s(L+M)}{sC}} \\ Z_{0o} &= \sqrt{\frac{R+s(L-M)}{s(C+2C_C)}} \end{aligned} \tag{4}$$

In the generic solution of (2), $e^{-\gamma z}$ terms represent waves traveling in +z direction and $e^{-\gamma z}$ terms represent waves traveling in $-z$ direction. The first term $A_1e^{-\gamma_e z}$ in the expression of V_1 and V_2 in (2) represents a voltage wave traveling in the +z direction with propagation constant γ_e and the second term $A_2e^{\gamma_e z}$ represents the corresponding reflected wave traveling in the reverse direction. Similarly, third and fourth terms represent similar traveling waves but with a different constant γ_o.

The above result shows that coupled lines have two modes of propagation with two different propagation constants and two different characteristic line impedances. The interesting implication of this observation is that the solution of two coupled lines can be viewed as the combination of the solutions of two single transmission lines. Physically, even mode represents the case when both lines switch in the same direction and odd mode represents the case when lines switch in opposite directions. Any signal traveling in the coupled transmission line system can be expressed as the superposition of these modes [10].

B. Coupled Noise Model

Based on the theory in Section 2.1, an accurate coupling noise model for on-chip interconnect can be developed. Figure 2 shows

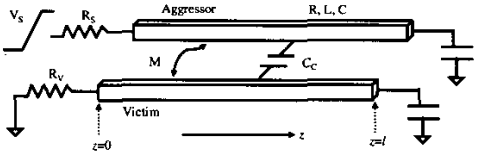

Fig 2: Coupled line configuration

two coupled interconnects where one line is switching and the other is quiet. The driver for the active line is replaced with a voltage ramp V_S in series with a Thevenin resistance R_S. For the quiet line, the driver is modeled as a linear resistance R_V connected to ground. Receivers at the far-end of the lines are modeled as lumped capacitive loads.

For global interconnect in typical CMOS designs, the receiver has a small input capacitance. From a transmission line point of view, a small capacitive load at the far-end of the line represents a large termination impedance. For example, a far-end capacitive load of 20fF at 1 GHz frequency corresponds to an impedance of around 8 KΩ. This impedance is significantly higher compared to the characteristic line impedance (which is normally around 50-60Ω). As a result, the far-end reflection coefficient in practical interconnects is around +1 [11].[2] This implies that any forward traveling wave is completely reflected at the far-end and the voltage at the far-end of the line is doubled due to the superposition of the incident voltage wave and the reflected reverse wave. In the generic solution given in (2), the amplitude of the reflected wave can be set equal to the incident wave and the solution of (2) can be simplified to

$$\begin{aligned} V_1 &= A_1(e^{-\gamma_e z} + e^{\gamma_e z}) + A_3(e^{-\gamma_o z} + e^{\gamma_o z}) \\ V_2 &= A_1(e^{-\gamma_e z} + e^{\gamma_e z}) - A_3(e^{-\gamma_o z} + e^{\gamma_o z}) \\ I_1 &= \frac{A_1}{Z_{Oe}}(e^{-\gamma_e z} - e^{\gamma_e z}) + \frac{A_3}{Z_{Oo}}(e^{-\gamma_o z} - e^{\gamma_o z}) \\ I_2 &= \frac{A_1}{Z_{Oe}}(e^{-\gamma_e z} - e^{\gamma_e z}) - \frac{A_3}{Z_{Oo}}(e^{-\gamma_o z} - e^{\gamma_o z}) \end{aligned} \tag{5}$$

At the near-end ($z = 0$), the active line (line 1) is driven by a voltage source V_S through a resistance R_S and the quiet line (line 2) is connected to ground through resistance R_V. Applying these boundary conditions to Equation 5 gives

$$\begin{aligned} \frac{V_S - V_1(z=0)}{I_1(z=0)} &= \frac{V_S - (A_1 + A_3)}{\left(\frac{A_1}{Z_{Oe}} + \frac{A_3}{Z_{Oo}}\right)} = R_S \\ \frac{-V_2(z=0)}{I_2(z=0)} &= \frac{-(A_1 - A_3)}{\left(\frac{A_1}{Z_{Oe}} - \frac{A_3}{Z_{Oo}}\right)} = R_V \end{aligned} \tag{6}$$

Solving the above set of equations for A_1 and A_3 gives

$$\begin{aligned} A_1 &= V_S \frac{Z_{Oe}(Z_{Oo} + R_V)}{(Z_{Oe} + R_S)(Z_{Oo} + R_V) + (Z_{Oe} + R_V)(Z_{Oo} + R_S)} \\ A_3 &= V_S \frac{Z_{Oo}(Z_{Oe} + R_V)}{(Z_{Oe} + R_S)(Z_{Oo} + R_V) + (Z_{Oe} + R_V)(Z_{Oo} + R_S)} \end{aligned} \tag{7}$$

[2] The analysis can be easily extended to the cases with large capacitive loads by considering a far-end reflection coefficient different than +1.

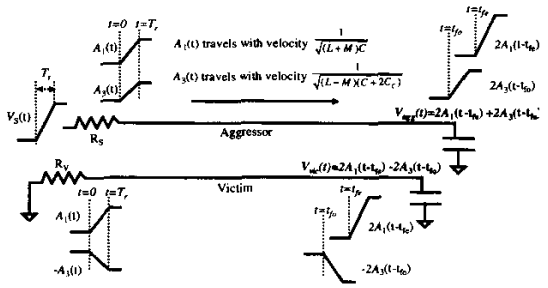

Fig 3: Far-end waveform computation in coupled transmission lines

Now, let us first consider the case of lossless lines only. We will consider losses in Section 3. For lossless lines, the term $e^{-\gamma_e z}$ in (5) simplifies to $e^{-s\left(z\sqrt{C(L+M)}\right)}$. This simplified term in the s-domain corresponds to a time delay of $z\sqrt{C(L+M)}$ in the time domain. Similarly, the exponential term for odd-mode corresponds to a time delay of $z\sqrt{(C+2C_C)(L-M)}$. Hence, any voltage step generated at the near-end in lossless coupled lines travels without any attenuation and distortion. For line length l, the step propagating with the even mode constant arrives at the far-end after an even time of flight t_{fe} and the step propagating with the odd mode constant arrives at the far-end after an odd time of flight delay t_{f0}.

$$t_{fe} = l\sqrt{C(L+M)} \qquad (8)$$
$$t_{fo} = l\sqrt{(C+2C_C)(L-M)}$$

Based on the above theory, the far-end waveforms in coupled lossless lines can be computed by performing the following steps:

- Given an input voltage ramp $V_S(t)$, compute the even and odd voltage ramps $A_1(t)$ and $A_3(t)$ using Equation 7.
- The voltage ramp $A_1(t)$ arrives at the far-end after t_{fe} and the voltage ramp $A_3(t)$ arrives at the far-end after t_{f0} delay.
- Due to a reflection coefficient of +1, both the voltage ramps are doubled at the far-end.
- The far-end waveforms for active and quiet lines can be computed by superposition of the doubled voltage ramps. In the active line, both even and odd modes are positive while in the quiet line the even mode is positive and the odd mode is negative.
- Reverse traveling waves can get reflected at the near-end and add to the far-end waveforms after three time of flight delays.

The above flow is explained in Figure 3. The figure shows that voltage steps $A_1(t)$ and $A_3(t)$ are generated at the near-end of the lines. These steps travel with different velocities and arrive at the far-end after different time delays. The output voltage waveforms can then be computed by:

$$V_{agg}(t) = 2A_1(t-t_{fe}) + 2A_3(t-t_{fo}) \qquad (9)$$
$$V_{vic}(t) = 2A_1(t-t_{fe}) - 2A_3(t-t_{fo})$$

Here, $V_{agg}(t)$ and $V_{vic}(t)$ are the waveforms at the output of aggressor and victim respectively.

Now that we have discussed the theory of coupling noise, we can use the above concepts to analyze noise waveforms. Let us consider the case of inductive and capacitive coupling separately.

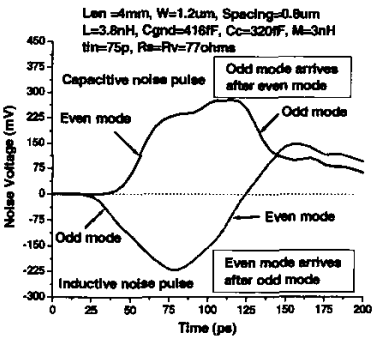

Fig 4: Typical noise waveforms for capacitive and inductive coupling noise explained using even-odd mode theory.

The even and odd mode characteristic impedances and times of flight for capacitive and inductive coupling are given by the following expressions.

For capacitive coupling only:

$$t_{fe} = l\sqrt{CL} \quad \text{and} \quad Z_{0e} = \sqrt{\frac{L}{C}} \qquad (10)$$
$$t_{fo} = l\sqrt{(C+2C_C)L} \qquad Z_{0o} = \sqrt{\frac{L}{(C+2C_C)}}$$

Similarly for inductive coupling only:

$$t_{fe} = l\sqrt{C(L+M)} \quad \text{and} \quad Z_{0e} = \sqrt{\frac{(L+M)}{C}} \qquad (11)$$
$$t_{fo} = l\sqrt{C(L-M)} \qquad Z_{0o} = \sqrt{\frac{(L-M)}{C}}$$

Capacitive coupling noise has positive polarity while inductive coupling noise has negative polarity. This can be explained by the time of flight expressions in Equations 10 and 11. For pure capacitive coupling, the even mode time of flight is less than the odd mode time of flight. Hence, the even mode voltage step arrives at the far-end before the odd mode step. Since even mode is positive and odd mode is negative, hence pure capacitive coupling results in a positive noise pulse. On the other hand, for pure inductive coupling the negative odd mode step travels faster than the positive even mode step, thereby resulting in a negative polarity noise pulse. Also, the even characteristic impedance is always larger than the odd characteristic impedance; thus the voltage step due to the even mode is bigger than the odd mode step. These observations are summarized in Figure 4 for capacitive and inductive noise waveforms in a 4 mm coupled line.

C. Noise Model for Different Line Parasitics

Now we consider the case of two coupled lines with different line parasitics. The configuration considered is the same as in Figure 2. The line parasitics per unit length for the active line (line 1) are R_1, L_1, and C_1 and those for the quiet line are R_2, L_2, and C_2. The differential equations in this case are given by

$$-\frac{\partial V_1}{\partial z} = (R_1 + sL_1)I_1 + sMI_2 \qquad -\frac{\partial I_1}{\partial z} = s(C_1 + C_C)V_1 - sC_CV_2$$
$$-\frac{\partial V_2}{\partial z} = (R_2 + sL_2)I_2 + sMI_1 \qquad -\frac{\partial I_2}{\partial z} = s(C_2 + C_C)V_2 - sC_CV_1 \qquad (12)$$

The generic solution for this set of differential equations (considering a far-end reflection coefficient of +1) is given by

$$\begin{aligned} V_1 &= A_1(e^{-\gamma_e z}+e^{\gamma_e z})+A_3(e^{-\gamma_o z}+e^{\gamma_o z}) \\ V_2 &= A_2(e^{-\gamma_e z}+e^{\gamma_e z})+A_4(e^{-\gamma_o z}+e^{\gamma_o z}) \\ I_1 &= \frac{A_1}{Z_{0e1}}(e^{-\gamma_e z}-e^{\gamma_e z})+\frac{A_3}{Z_{0o1}}(e^{-\gamma_o z}-e^{\gamma_o z}) \\ I_2 &= \frac{A_2}{Z_{0e2}}(e^{-\gamma_e z}-e^{\gamma_e z})+\frac{A_4}{Z_{0o2}}(e^{-\gamma_o z}-e^{\gamma_o z}) \end{aligned} \quad (13)$$

For simplicity, let us consider the case of lossless lines (this assumption will be addressed in Section 3). Even and odd mode propagation constants γ_e and γ_o are given by

$$\begin{aligned} \gamma_e &= s\sqrt{\frac{(a_1+a_2)+\sqrt{(a_1-a_2)^2+4b_1b_2}}{2}} \\ \gamma_0 &= s\sqrt{\frac{(a_1+a_2)-\sqrt{(a_1-a_2)^2+4b_1b_2}}{2}} \end{aligned} \quad (14)$$

where

$$\begin{aligned} a_1 &= L_1(C_1+C_C)-MC_C & a_2 &= L_1(C_2+C_C)-MC_C \\ b_1 &= -L_1C_C+M(C_2+C_C) & b_2 &= -L_2C_C+M(C_1+C_C) \end{aligned} \quad (15)$$

For symmetric lines, a_1=a_2 (=a) and b_1=b_2 (=b), and the expressions for even and odd mode propagation constants in Equation 14 reduce to

$$\begin{aligned} \gamma_e &= s\sqrt{a+b} = s\sqrt{C(L+M)} \\ \gamma_o &= s\sqrt{a-b} = s\sqrt{(C+2C_C)(L-M)} \end{aligned} \quad (16)$$

In the solution of (13), the coefficients are related as

$$\begin{aligned} \frac{A_1}{A_2} &= \frac{(a_1-a_2)+\sqrt{(a_1-a_2)^2+4b_1b_2}}{2b_2} \\ \frac{A_3}{A_4} &= \frac{(a_1-a_2)-\sqrt{(a_1-a_2)^2+4b_1b_2}}{2b_2} \end{aligned} \quad (17)$$

Again for symmetric lines, A_2=A_1 and A_4=-A_3, and (13) reduces to the equation for symmetric lines.

Another difference for asymmetric lines is that even and odd mode characteristic impedances for the two lines are different. These impedances are given by

$$\begin{aligned} Z_{0e1} &= \frac{s(L_1L_2-M^2)}{\gamma_e(L_2-\frac{A_2}{A_1}M)} & Z_{0e2} &= \frac{s(L_1L_2-M^2)}{\gamma_e(L_2-\frac{A_1}{A_2}M)} \\ Z_{0o1} &= \frac{s(L_1L_2-M^2)}{\gamma_o(L_2-\frac{A_4}{A_3}M)} & Z_{0o2} &= \frac{s(L_1L_2-M^2)}{\gamma_o(L_2-\frac{A_3}{A_4}M)} \end{aligned} \quad (18)$$

Applying the boundary condition in a similar way as for symmetric lines, the voltage steps traveling on the quiet line can be computed as

$$A_2 = \frac{V_S}{\left(\frac{A_1}{A_2}\right)\left(\frac{Z_{0e1}+R_S}{Z_{0e1}}\right)-\left(\frac{A_3}{A_4}\right)\left(\frac{Z_{0e2}+R_V}{Z_{0o2}+R_V}\right)\left(\frac{Z_{0o2}}{Z_{0e2}}\right)\left(\frac{Z_{0o1}+R_S}{Z_{0o1}}\right)}$$

$$A_4 = \frac{V_S}{\left(\frac{A_3}{A_4}\right)\left(\frac{Z_{0o1}+R_S}{Z_{0o1}}\right)-\left(\frac{A_1}{A_2}\right)\left(\frac{Z_{0o2}+R_V}{Z_{0e2}+R_V}\right)\left(\frac{Z_{0e2}}{Z_{0o2}}\right)\left(\frac{Z_{0e1}+R_S}{Z_{0e1}}\right)} \quad (19)$$

The overall flow for computing noise waveforms in asymmetric lines is the same as that in symmetric lines. For a given input ramp to the active line, the two voltage ramps A_2(t) and A_4(t) are generated on the quiet line. The two ramps propagate at different speeds and arrive at far-end of the line after t_{fe} and t_{f0} time of flights respectively. These waveforms get doubled at the far-end and the noise waveform is then computed by the superposition of these two ramps. The times of flight are given by

$$\begin{aligned} t_{fe} &= l\sqrt{\frac{(a_1+a_2)+\sqrt{(a_1-a_2)^2+4b_1b_2}}{2}} \\ t_{f0} &= l\sqrt{\frac{(a_1+a_2)-\sqrt{(a_1-a_2)^2+4b_1b_2}}{2}} \end{aligned} \quad (20)$$

III. Validation Of The Model

In this section, we test the model by comparing it to HSPICE simulations. We consider the testcases with realistic interconnect topologies (for example, maximum interconnect length considered is 4mm because wires longer than 4mm are often broken into shorter wires by repeater insertion). Far-end capacitive loading of 30fF is considered in simulations. Line parasitics are extracted using the commercial extraction tool Raphael. A two-layer orthogonal power grid structure with 50μm pitch and 10μm linewidth is used in inductance extraction. All simulations use a 0.13μm 1.2V technology.

Figure 5 shows the comparison between model and HSPICE for three arbitrarily chosen line configurations. In computing the model waveforms, the first set of reflections from the near-end were also considered. For one of these cases, we swept the aggressor input transition time from 20ps to 200ps. Figure 6 compares the measured and calculated peak noise values as a function of input transition time. In all these testcases, line resistance was not considered.

Now, we discuss the effect of line resistance on noise waveforms. Figure 7 shows HSPICE waveforms for three different line resistances. The figure shows that as line resistance increases, the noise peak reduces. This is due to the fact that with resistance, the voltage steps traveling along the line undergo attenuation and dispersion. Hence the voltage steps arriving at the far-end of the line are smaller and have larger rise times. This causes noise pulses in the lossy lines to be smaller and wider as compared to those in lossless line. This is helpful since the noise peak values obtained using a lossless approximation can be safely assumed to be pessimistic.

Including resistance in the transmission line analysis adds significant complexity to the problem and the resulting equations fail to provide much physical insight. For simplicity, a low loss approximation is used to include the effect of line resistance in the above lossless model. In a low loss approximation (R<$2Z_0$), a voltage step traveling along a transmission line of characteristic impedance Z_0 is attenuated by a factor of $e^{-\frac{R}{2Z_0}}$ [10]. Based on this theory, positive and negative noise peak values in lossy lines can be computed as

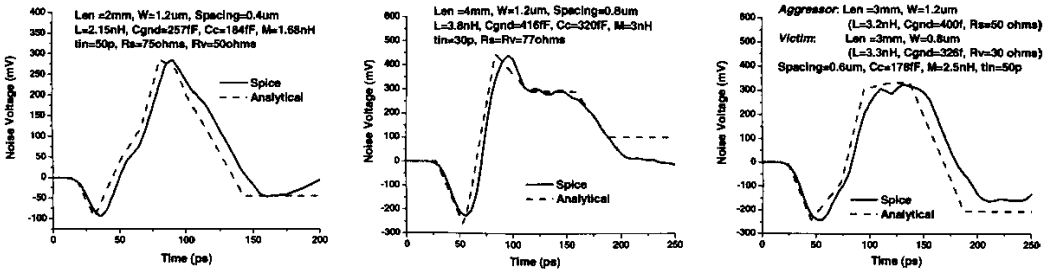

Fig 5: Noise waveforms using HSPICE and analytical model

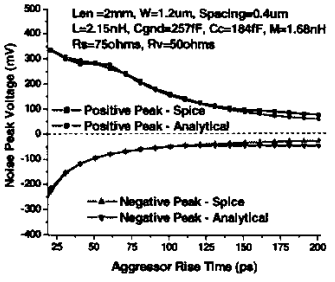

Fig 6: Measured and calculated noise peak for various input aggressor transition time

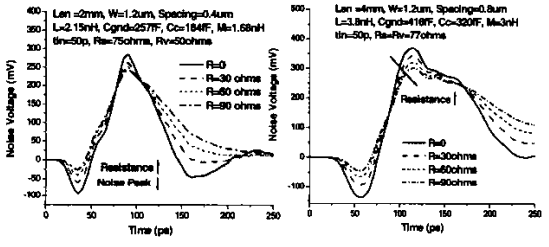

Fig 7: Noise waveforms for three different line resistances.

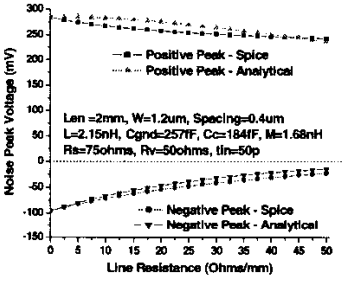

Fig 8: Measured and calculated noise peak for various line resistances.

$$V_{lossy}^{-} = V_{lossless}^{-} \times e^{-\frac{R}{2Z_{0e}}} \qquad (21)$$

$$V_{lossy}^{+} = V_{lossless}^{-} \times e^{-\frac{R}{2Z_{0e}}} + (V_{lossless}^{+} - V_{lossless}^{-}) \times e^{-\frac{R}{2Z_{0e}}}$$

Here, V^{-} and V^{+} represent the negative and positive peaks respectively.

Table I: Error bins in peak noise estimation for 532 testcases

Error bins	<5%	<10%	<15%
% of testcases	52%	81%	90%

Figure 8 shows HSPICE and analytical results obtained by sweeping line resistance. The figure shows that both negative and positive noise peak decrease with line resistance and this effect is captured well by the analytical equations.

Finally, we tested the complete analytical model including the lossy approximation by sweeping line length from 1mm to 4mm and linewidth from 0.8μm to 3.2μm. Line to line spacing was swept from 0.4μm to 1μm. We also varied input transition time from 50ps to 150ps. Table I shows the error bins in peak noise estimation for these 532 testcases covering different wire topologies. The table shows that the model works extremely well with 81% of the testcases showing less than 10% error.

The average error in noise peak estimation over entire set of 532 testcases was 6.5%. On examining the testcases, we found that the cases with large errors correspond to long and narrow wires. Such wires are not common in practical designs because they have high line resistance and hence are buffered more often to reduce RC delay.

IV. Effect of Line Parameters on Coupling Noise

The analytical noise model proposed in the previous sections can be used to quickly screen for logic (or timing) failures due to coupling noise during physical design. Once a failure is detected, the routing should be modified to ensure proper operation. One way to manage coupling noise is by controlling line parasitics which in turn can be controlled by wire sizing and spacing as well as shield line insertion. In this section, we study the effect of changing line parasitics on inductive and capacitive noise. Before we study these effects in detail, we highlight two observations from the theory discussed in Section 2.

- If the difference between even mode and odd mode times of flight increases, then peak noise grows. This is due to the fact that even and odd mode voltage ramps are in the opposite direction. Hence if the difference in their arrival times is larger, then the voltage step due to the first mode (mode that arrives first at the far-end) can rise to a higher value before being pulled down by the second mode.

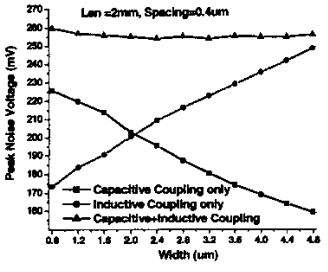

Fig 9: Absolute peak noise voltage vs. linewidth for capacitive, inductive and capacitive + inductive coupling.

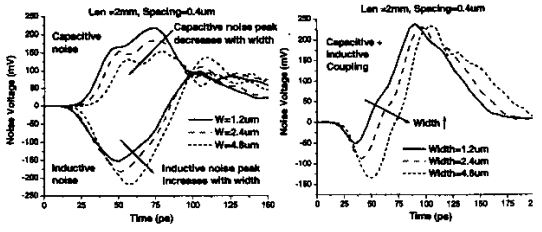

Fig 10: Noise waveforms for capacitive and inductive coupling (left) and for capacitive + inductive coupling (right) for three different linewidths.

- If the victim driver resistance is fixed, then the height of the even step increases as the ratio $\frac{Z_{0e}}{Z_{0e}+R_S}$ increases. Similarly the height of the odd step increases with a rise in the ratio $\frac{Z_{0o}}{Z_{0o}+R_S}$.

A. *Effect of Linewidth (Ground Capacitance) on Noise*

For physical design tools, linewidth is an important parameter during wire optimization because it has a significant effect on both line resistance and ground capacitance. In this section, we consider the effect of linewidth on coupling noise. We consider two coupled lines where each line is 2mm long and the spacing between them is fixed at 0.4μm. Linewidth of both wires is swept from 0.8μm to 4.8μm in steps of 0.4μm. For each width, line parasitics were extracted using commercial extraction tool Raphael.

For each width, peak noise is computed using the model proposed in this paper. We consider three cases - capacitive coupling only, inductive coupling only, and both coupling together. As linewidth increases, the ground capacitance of the line increases. With increased line capacitance, the aggressor transition time slows down considerably. Hence for a fair comparison; the aggressor driver resistance was varied such that the RC product of driver resistance and total line capacitance remains constant. The input transition time to the aggressor is 50ps, victim diver resistance is 50Ω, and the aggressor driver resistance varies from 100Ω to 42Ω. Figure 9 shows the absolute peak noise voltage as a function of linewidth. The figure shows that as linewidth increases, noise peak due to capacitive coupling reduces as expected while the noise peak due to inductive coupling increases. The actual noise peak while considering both forms of coupling was not very sensitive to the width. This is an interesting result because increasing linewidth is traditionally considered a useful noise avoidance technique but it actually worsens inductive noise. We also simulate the full noise waveforms for three different widths in HSPICE. Figure 10 shows the waveforms for capacitive, inductive and both coupling cases for three different linewidths.

The above behavior of capacitive and inductive noise can be explained based on the theory discussed in the paper. For capacitive coupling, the even mode time of flight is given by $l\sqrt{LC}$ while the odd mode time of flight is given by $l\sqrt{L(C+2C_c)}$. Now, as ground capacitance C increases the difference between even and odd mode times of flight reduces. This causes capacitive noise to reduce with width. For inductive coupling, the difference between even mode time of flight ($l\sqrt{(L+M)C}$) and the odd mode time of flight ($l\sqrt{(L-M)C}$) increases with a rise in ground capacitance C. Hence, contrary to capacitive coupling, inductive coupling noise peak increases with linewidth. It should be noted that with increased ground capacitance, both even and odd mode characteristic impedances reduce. If driver resistance is fixed, then this will result in reduced heights for even and odd mode steps. However, in our experiment, aggressor driver resistance was decreased to maintain a fixed RC product; making the effect of change in characteristic impedances on noise peak less significant.

B. *Effect of Self Inductance on Noise*

Unlike capacitance, inductance is only a weak function of line geometry and is primarily controlled by the position of current return paths. With the increasing significance of inductance, it is required that physical design tools consider inductance during shield insertion and power grid specification. In this section, we study the effect of changing self inductance on noise. A similar setup as in Section 4.1 is used. In the experiment we consider 2 mm long lines with 1.2μm width and 0.4μm spacing. Aggressor and victim driver resistances are 100Ω and 50Ω respectively and input transition time is 50ps. Instead of using extracted self inductance values, it is swept from 2nH to 5nH.

Figure 11 shows absolute peak noise voltages as a function of self inductance calculated using the model. The figure shows that as self inductance increases, noise peak due to capacitive coupling increases significantly. Noise peaks while considering inductive coupling only and the total noise considering both couplings were not very sensitive to the width. This is an interesting result since we find that increasing self inductance affects capacitive noise more than inductive noise. Also, consider that with capacitive coupling, when the ratio of coupling capacitance to ground capacitance is reduced, the capacitive noise reduces. Along the same lines for inductance, we might speculate that increasing the self inductance should reduce the mutual to self inductance ratio and hence reduce inductive noise. However, in our experiment we found that for increasing self inductance, the noise peak due to inductive coupling increases slightly. Figure 12 shows HSPICE waveforms for capacitive, inductive, and total coupling cases for three different self inductances.

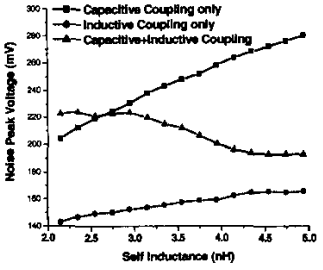

Fig 11: Absolute peak noise voltage vs. line self inductance for capacitive, inductive and capacitive + inductive coupling.

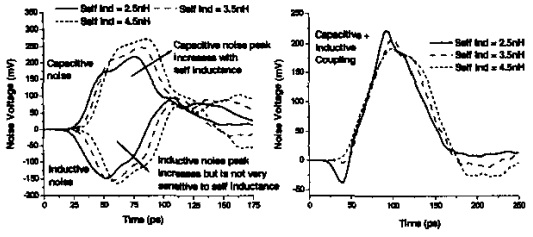

Fig 12: Noise waveforms for capacitive and inductive coupling (left) and for capacitive + inductive coupling (right) for three different line self inductances.

This behavior can again be explained by the two observations made in the beginning of this section. For capacitive noise, as self inductance is increased the difference between even ($l\sqrt{LC}$) and odd mode times of flight ($l\sqrt{L(C+2C_c)}$) increases. Also, with self inductance, even and odd mode characteristic impedances also increase causing capacitive noise to increase significantly. For inductive noise, the difference between even mode time of flight ($l\sqrt{(L+M)C}$) and the odd mode time of flight ($l\sqrt{(L-M)C}$) reduces but characteristic impedances increase. Due to the conflicting impact of these two factors on noise, the inductive noise peak is fairly insensitive to self inductance.

C. *Effect of Spacing on Noise*

Finally, we study the effect of spacing on noise. A similar setup as in Section 4.1 is used. Line to line spacing is swept from 0.4μm to 3.2μm in steps of 0.4μm. For each spacing, line parasitics are extracted and coupling noise behavior is computed using the new RLC model. Figure 13 shows the absolute peak noise voltages as a function of spacing. The figure shows that with increased spacing, noise peaks due to both capacitive and inductive coupling reduce. As expected, the reduction in inductive noise is not as significant as that in the capacitive noise. This is due to the fact that with spacing, the coupling capacitance reduces more rapidly as compared to the mutual inductance. The figure also shows that for large spacings, the total noise is dominated by inductive coupling only. This implies that only small increases in spacing are useful (e.g., in this case from 0.4μm to 0.8μm) since beyond this point noise reductions have saturated due to the presence of mutual inductance.

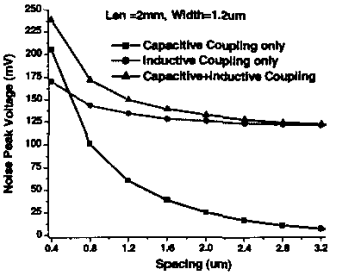

Fig 13: Absolute peak noise voltage vs. line to line spacing for capacitive, inductive and capacitive + inductive coupling.

V. Conclusions

In this paper, we have proposed a simple crosstalk noise model for coupled RLC interconnects. Our results show that the model captures the noise waveform shape well with an average error of 6.5% for noise peak over a wide range of testcases. The model is then used to investigate sensitivities of *total* noise to layout parameters such as width, spacing, power grid granularity. Our analysis shows that traditional capacitive coupling based physical design noise optimizations are not efficient when both capacitive and inductive coupling are considered together.

References

[1] Y. I. Ismail and E. G. Friedman, *On-Chip Inductance in High Speed Integrated Circuits*, Kluwer Acad. Publishers, 2001.

[2] C. K. Cheng, J. Lillis, S. Lin and N. Chang, *Interconnect Analysis and Synthesis*, John Wiley & Sons, 2000.

[3] A. Deutsch *et al.*, "The Importance of Inductance and Inductive Coupling for On-Chip Wiring", *Proc. Topical Meeting on Electrical Performance of Electrical Packaging*, pp. 53-56, 1997.

[4] D. Sylvester and K. Shephard, "Electrical Integrity Design and Verification for Digital and Mixed-Signal Systems on a Chip", *Tutorial - Intl. Conf. Computer Aided Design*, 2001.

[5] K. T. Tang and E. G. Friedman, "Interconnect Coupling Noise in CMOS VLSI Circuits", *Proc. Intl. Symp. on Physical Design*, pp. 48-53, 1999.

[6] L. He, N. Chang, S. Lin and O. S. Nakgawa, "An Efficient Inductance Modeling for On-Chip Interconnects", *Proc. Custom Integrated Circuits Conference*, pp. 457-460, 1999.

[7] L. Yin and L. He, "An Efficient Analytical Model of Coupled On-Chip RLC Interconnects", *Proc. Asia South Pacific Design Automation Conference*, pp. 385-390, 2001.

[8] J. Davis and J. Meindl, "Compact Distributed RLC Interconnect Models – Part II: Coupled Line Transient Expressions and Peak Crosstalk in Multilevel Networks", *IEEE Trans. Electron Devices*, pp. 2078-2087, Nov. 2000.

[9] K. C. Gupta, *Microstrip Lines and Slotlines*, Boston Artech House, 1996.

[10] H.B. Bakoglu, *Circuits, Interconnections, and Packaging for VLSI*, Addison-Wesley, 1990.

[11] B. Young, *Digital Signal Integrity*, Prentice Hall, 2001